Isotropic to nematic transition in solutions of cylindrical PB-PEO block copolymer micelles close to a wall

Peter Lang Lutz Willner, Wim Pyckhout-Hintzen and Rumen Krastev*[a].

Forschungszentrum Jülich, IFF, 52425 Jülich, Germany

[a]Hahn-Meitner-Institut, Glienicker-Straße 100, 14109 Berlin, Germany

* Author to whom correspondence should be addressed; electronic mail: p.lang@fz-juelich.de

RECEIVED DATE (to be automatically inserted after your manuscript is accepted if required according to the journal that you are submitting your paper to)

Abstract The influence of a flat interface on the isotropic to nematic (I/N) phase transition was investigated for aqueous solutions of cylindrical micelles of polybutadiene-poly(ethylene oxide) block copolymers using specular neutron reflectivity. While the I/N-transition in the bulk occurs at the solute volume fraction $\phi_{N/I}$, we observed the formation of a condensed layer close to a silicon single crystal interface at volume fractions of about $\phi_i \approx 0.85 \times \phi_{I/N}$. The thickness of this layer does not vary if the solute fraction is changed, while it's density increases drastically within a very narrow range of volume fractions. This observation is interpreted as the formation of a nematicaly ordered layer which is induced by the interface.

Introduction

In low molar mass systems the effect of surface condensation and accompanying wetting phenomena has been investigated in great detail during the last two decades. For a variety of low molar mass single and multi component systems it has been observed that order to disorder transitions are shifted by the presence of a flat interface, in such a way that the higher ordered phase is stable close to the interface, while in the bulk the system is in the less ordered state at the same thermodynamic conditions [1-7]. However the wetting behavior of the ordered phase depends very sensitively on the chemical structure and the molecular interaction of the respective compounds. A classical example of surface condensation with complete wetting is the formation of smectic films on top of nematic liquid cystals [2,8], while surface crystallization with incomplete wetting has been observed for higher n-alkanes [3].

Similar to low molar mass mesogens, suspensions of colloidal rods also form liquid crystalline phases at higher volume fraction. The phase transition from the isotropic to the nematic phase (I/N) has been studied for many years. In his pioneering paper in 1949, Onsager formulated the first microscopic theory of the isotropic-nematic phase transition [9] and it can be said that at present the phase behavior of a homogeneous system of hard rods is well understood. On the other hand, it is quite poorly understood how the presence of an interface influences the phase behavior of a suspension of rods. Only recently have a few theoretical and simulation studies been devoted to this subject [10,11]. In these studies, it is predicted that the interface between a hard wall and an isotropic fluid of hard rods induces two kinds of pretransitional ordering effects, i.e. an uniaxial to biaxial transition at low volume fractions with subsequent wetting of the interface by the nematic phase. The nematic layer gives rise to a distinct concentration profile in which the rod concentration next to a wall is significantly higher than the concentration of the rods in the isotropic bulk. These studies are concerned with monodisperse rigid cylinder systems, which interact by a hard body potential. An approach which takes into account a finite flexibility of the cylinders was published by Chen et al.[12,13] which also predicts the formation

of a nematically ordered layer close to a wall, while the bulk material is still in the isotropic state. On the other hand, there are only very few systematic experimental reports on interface induced ordering phenomena in colloidal suspensions[14,15]. In particular experiments of the isotropic to nematic pre-transition of colloidal cylinder suspensions are completely absent. In this contribution we present a first investigation of such a system, namely aqueous solutions of the amphiphilic polybutadiene-poly(ethylene oxide) block copolymers (PB-PEO) against a silicon single crystal interface.

There has been a large number of publications on the micellar morphologies and the structure of liquid crystalline meso—phases formed in block copolymer solutions and a corresponding large number of morphologies has been reported. In the field of water based solutions, Förster et al were the first to show that the morphology of polyelectrolyte micelles can be tuned varying the respective block lengths and the ionic strength of the solvent[16,17]. Besides polyelectrolyte based copolymers, there are only very few types of block copolymers, which have been studied in aqueous solution. They may be divided into three groups, which are all based on PEO blocks as the hydrophilic part. The major part of the contributions report on solutions of PEO-polypropyleneoxide-PEO triblock coplymers, in which a wealth of different structures were observed[18,19]. A second group is concerened with polymers, which form aggregates that have glassy cores due to the high glass transition temperature of the hydrophobic moiety[20-23]. In this case desired morphologies can be tailored by elaborate processing. Finally there are block copolymers with polyisoprene (PI-PEO)[24], polyethylenepropylene (PEP-PEO)[25-28] and polybutadiene[29-33] as the water insoluble part, which all have low glass transition temperatures. In these cases the micellar shape is determined by the length ratio of the blocks, the overall chain length of the polymer and the solute concentration.

At small degrees of polymerization PB-PEO block copolymers dissolve easily in water to form aggregates with spherical, cylindrical or bilayer morphology. Only at large molar mass of the constituting unimers more complex structures such as Y-junctions and networks are observed[33]. For low molar mass copolymers with balanced block length the formation of cylindrical micelles is favored.

These micelles attain nematic order at solute volume fraction of about five to ten percent and hexagonal order at higher concentrations [29, 30].

We have synthesized two short chained PB-PEO block copolymers, h-PB1,4-h-PEO and d-PB1,4-d-PEO, by anionic polymerization with similar molar mass of the respective blocks and predominantly 1,4 microstructure in the polybutadiene. The micellar shape in aqueous solution was analyzed by static light scattering (SLS) and small-angle neutron scattering (SANS). For the analysis of SLS-data the scattered intensity at a given concentration c and scattering vector $Q = (4\pi n / \lambda_0)\sin(\Theta/2)$ are converted to the quantity $Kc/R(Q)$, where n is the refractive index of the solution, Θ is the scattering angle, λ_0 is the wavelength of the incident light in vacuum, c is the solute concentration in units of g/mL and K is an optical contrast factor. If the scattered intensity may be factorized into a structure contribution $S(Q,c)$ and a particle contribution $P(Q)$, one can write

$$\frac{Kc}{R(Q)} = \frac{1}{M_W S(Q,c) P(Q)} \equiv \frac{1}{M_{app}(c) P(Q)} \qquad (1)$$

where M_W is the particle molar mass and $M_{app}(c)$ the so called apparent molar mass at a given concentration. Since $P(Q=0)=1$, extrapolation of $Kc/R(Q)$ to zero scattering vector yields $M_{app}(c)$. For sufficiently dilute solutions $S(Q,c)$ can be expressed as a second order virial expansion in c and consequently $1/M_{app}(c)$ may be extrapolated linearly to zero concentration. According to Zimm [34] this yields $1/M_W$, as the intercept and the slope is $2A_2$ with A_2 the second osmotic virial coefficient.

Consequently $S(Q=0,c)$, M_W, and A_2 can be obtained from SLS experiments. These quantities can be used to obtain qualitative information on the shape of the scattering particles, if the variation of $1/S(Q=0,X)$, with $X=c2A_2M_W$ as the reduced concentration, is analyzed. [35].

More quantitative information on the shape of micelles are available from SANS-experiments. If experimental scattering data, collected from sufficiently dilute samples, can be analyzed by non linear least squares fitting to an appropriate model function for the particle scattering factor, $P(Q)$. The micrographs of PB-PEO micelles published by Won et al[29] strongly suggest that the micellar cylinders have a significant flexibility, which must be taken into account in the analysis of SANS data.

In the recent years there have been two approaches to construct a particle scattering factor for semi-flexible cylindrical particles [36,37], which both make use of the fact, that the length scales of the micellar contour length, L_c, and the cross-section radius, R_{cs}, are well separated. In this case $P(Q)$ may be factorized into a length contribution $P(Q,L_c,b,U)$ and a contribution of the cross-section. $P(Q,R_{cs})$, where b is the statistical Kuhn-segment length [38], and U is the length polydispersity index. While Pedersen et al. developed a semi-empirical expression based on simulation results for $P(Q,L_c,b,U)$, Menge et al. used the expression given earlier by Koyama [39]. In this contribution, we used the method by Menge et al for reasons which are discussed in their paper.

A very powerful tool to investigate the effect of the Si-interface on the N/I transition is neutron reflectivity (NR) [40]. In NR one measures the specular reflectivity of neutrons as a function of the scattering vector $Q_z = (4\pi/\lambda)\sin\alpha$ normal to the surface, where α is the reflection angle. The reflectivity $R(Q_z)$ is related to the scattering length density profile in the direction normal to the surface, $\rho(z)$. A perfectly smooth interface between two half-spaces, each with constant $\rho(z)$ up to the interface, yields a monotonically decaying $R(Q_z)$ vs Q_z curve, while the presence of a layer with different scattering length density adjacent to the interface causes an undulation of the reflectivity curve. The period of this undulation is related to the layer thickness, while it's amplitude is related to the scattering length density of the layer. For the quantitative analysis of NR-data a model independent method [41,42] can be applied as well as the commonly used so called multi-box (or slab) model [43] in which the profiles are analyzed in terms of box height, box density and the roughness parameter of the interface between adjacent boxes.

The paper is organized as follows. First we present the bulk scattering experiments on PB-PEO in aqueous solution and their analysis. In the main part of the paper we report NR-data from the interface between a Si-single crystal and solutions of PB-PEO with different scattering contrasts. The data are analyzed in terms of the thickness and density of a condensed layer close to the interface. In the discussion we compare our experimental observations to theoretical predictions for hard rod fluids and solutions of semi-flexible liquid crystalline polymers.

Experimental Section

Synthesis of the blockcopolymers h-PB1,4-h-PEO and d-PB1,4-d-PEO was accomplished by anionic polymerization. The polymerization was realized by a two step process, because each block requires different reaction conditions. At first two polybutadienes with a high degree of 1,4-microstructure were synthesized from 1,3-butadiene-d_6 (Chemotrade, Leipzig, Germany, 98% d) and 1,3-butadiene-h_6, respectively, using t-butyllithium as initiator and benzene as reaction solvent. The living polymers were end capped by the addition of an excess amount of either ethylene oxide-d_4 (CDN Isotopes, Quebec Canada, 99,8% d) or ethylene oxide-h_4, and were terminated with acetic acid. Since no propagation of EO takes place with lithium as counterion in nonpolar media, the chain end is functionalized by exclusively one hydroxyethyl group. The two polymers, h-PB1,4-OH and d-PB1,4-OH, were precipitated in methanol and dried in high vacuum until any kind of volatile impurity was removed. In the second polymerization step, naphthalene potassium was used to convert the PB-OH polymers into the macroinitiators h-PB1,4-OK and d-PB1,4-OK. These were used to polymerize EO-h_4 and EO-d_4 in THF at 50°C for two days. The living polymers were terminated with acetic acid and then precipitated twice in acetone at –20°C. A more detailed description of the synthetic procedure is given elsewhere [44].

The PB1,4-OH precursor polymers were characterized by size exclusion chromatography (SEC) at 30°C using a Waters 150-CVplus chromatograph combined with a Viscotek Model 300 triple detector array. Four ultra-styragel columns covering a nominal porosity range from 100Å to 10^4Å were used with tetrahydrofuran (THF) as eluant at a flux rate of 1mL/min. The system was conventionally calibrated with narrow molecular weight polystyrene standards and, in addition, a set of well-defined polydiene standards were taken to generate a universal calibration curve. Polydispersities, M_w/M_n, were calculated from the conventional calibration curve, while molecular weights were extracted from universal calibration. Absolute molecular weight of the fully proteated polymer, h-PB1,4-OH, was determined by ^{1}H-NMR-spectroscopy using a Bruker AMX 300 instrument. The number average

molecular weight, M_n, was calculated by comparison of the signal intensities arising from the PB-repeat units with those from the 9 protons of the initiator group. From the ^{1}H-NMR spectrum the microstructure of the polymer was determined to consist of 88% 1,4- and 12% 1,2 –repeat units. For the deuterated polymer the same microstructure was assumed since the polymer was prepared under analogous conditions.

The block copolymers were examined by SEC at 30°C using a second chromatopgraphy set-up consisting of a Waters 150C instrument and four ultra-Styragel columns of constant pore size together with one column of continuous pore size covering an overall porosity range from 500Å to 10^5Å. The run conditions were 1mL/min flow of a mixture of THF and N,N-dimethylacetamide (90:10 by volume). Narrow molecular weight polystyrene standards were used for calibration. The elution peaks of both block copolymers reveal narrow molecular weight distributions without any sign of homopolymer contamination. Absolute molecular weight of the h-PEO-block in h-PB1,4-h-PEO was determined by ^{1}H-NMR. Based on the known molecular weight of the h-PB1,4 –OH block, M_n, was determined by relating the signal intensities of PB with the intensity of PEO-methylene units. The molecular weight of the d-PEO in the fully deuterated block copolymer was estimated on the basis of known d-PB1,4-OH molecular weight and comparison of the elution volumes of proteated and deuterated precursor and block copolymers. A summary of the molecular characteristics of the polymers is given in Table 1.

Table 1 Molecular characteristics of the blockcopolymers

	PB		PEO	
Blockcopolymer	M_n /g/mol	M_w/M_n [a]	M_n g/mol	M_w/M_n [a]
h-PB1,4-h-PEO	1600[b]; (1700[c])	1.06	1600[c]	1.05
d-PB1,4-d-PEO	1750[b]	1.06	1900[d]	1.03

[a] by conventional SEC, [b] by SEC with universal calibration, [c] by ^{1}H-NMR, [d] estimated from the comparison of the elution volumes of precursor and blockcopolymer.

Static Light Scattering experiments were performed on a series h-PB1,4-h-PEO solutions in H_2O, which were prepared by dilution of stock solution with a solute content of c = 5.25×10^{-3} g/mL. We used a commercial LS-apparatus by ALV-Laservertriebsgesellschaft, Langen, Germany which is equipped with a He/Ne Laser with a power output of 15 mW and a wavelength of λ_0=632 nm as the primary light source. The scattering angle was varied from 20° to 150° in 5° steps to cover a range of scattering vectors 4.59×10^{-4} Å^{-1}≤Q≤2.55×10^{-3} Å^{-3} nm^{-1} depending slightly on the concentration as the refractive index of the solution is n=n_0+c dn/dc. Here n_0 is the index of refraction of the pure solvent and dn/dc is the refractive index increment which was measured with the DR1 instrument from ALV. Reduced integrated excess intensities $R(Q)$ were derived from the relative scattered intensities $r(Q)$ = $i(Q)/I_0$ and converted to the quantity Kc/R(Q), where the contrast factor K was calculated according to the standard procedure, which is described in detail elsewhere [45]. Values of 1/S(Q=0) were determined by linear least squares fitting of plots of Kc/R(Q) vs. Q^2. Since Kc/R(Q) did not depend linearly on Q^2 in the whole experimental range, we used only the initial part of the curves for the fitting where a correlation coefficient better than 0.99 could be obtained. This was typically the range below Θ≤50° corresponding to Q^2≤1.25×10^{-6} Å^{-2}.

Small-Angle Neutron Scattering (SANS) data were collected on the KWS1 instrument at the FRJ2 reactor (20 MW), Forschungszentrum Jülich GmbH (FZJ). Neutrons were derived from a hydrogen cold source and monochromatized by a velocity selector. The mean de Broglie wavelength was set to λ_0= 7 Å with a full width spread of $\Delta\lambda/\lambda_0$=0.2. The instrument was equipped with a 64×64 Li-scintillation detector with a pixel size of 8×8 mm^2, which was positioned at three different sample-to-detector distances (2 m, 8 m and 20 m) to cover a range of scattering vectors 2×10^{-3} Å^{-1}≤Q≤0.15 Å^{-1} after radial averaging. Solutions with a polymer concentration of 1 mg/mL were measured in quartz cells with a path length of 1 mm. Sampling times were chosen such that the statistical error was smaller than 2 % at any scattering vector. Data reduction and calibration of intensities using Lupolene as a secondary standard, was achieved by FCJ standard procedures [46].

Neutron reflectivity experiments were run at the reflectometer V6 of BENSC at the Hahn-Meitner Institute, Berlin, Germany. A detailed description of the instrument is given elsewhere[47]. The neutron de Broglie wavelength was set to 4.66 Å by an array of single-crystal graphite monochromators in the white beam. The incoming beam cross-section profile was defined by two adjustable slits inserted between the monochromators and the sample. The scattered neutrons were recorded with a ^{3}He-detector. The primary intensity was monitored with a counter placed directly in the incident beam path.

Reflectivity scans were conducted on two dilution series, the first consisting of the proteated diblock copolymer dissolved in D_2O and the second of the deuterated diblock copolymer dispersed in a D_2O/H_2O-mixture. The composition of the isotopic water mixture was adjusted to match the scattering length density of single crystalline silicone (so-called null reflecting water). As sample cells we used Vespel troughs with a volume of 2.5×75×45 mm^3 which were covered with Si single-crystal with a size of 25×50×80 mm^3. Since single crystalline silicone is transparent for neutrons the reflectivity measurement from the solid/liquid interface could be performed in a $\alpha/2\alpha$ geometry where α is the sample angle and 2α is the detector angle with respect to the incident beam direction. Each reflectivity scan covered a range of scattering vectors from Q_z = 4.7×10^{-3}Å^{-1} to 0.155 Å^{-1} for the solutions of proteated diblock copolymer in D_2O. In the case of solutions of deuterated diblock copolymer in null reflecting water the incoherent background scattering was much higher, thus reducing the highest scattering vector at which a reasonable signal to noise ratio was observed to $Q_z \leq 0.0518$ Å^{-1}. The incident beam was collimated by the slit system to a rectangular cross-section of 0.5×40 mm^2 if $Q_z \leq 0.0518$ Å^{-1} and of 1.0×40 mm^2 elsewhere. Accordingly the resolution was $\Delta Q_z \approx 10^{-3}$ Å^{-1} in the low Q_z-range and $\Delta Q_z \approx 2\times10^{-3}$ Å^{-1} in the range above Q_z=0.0518 Å^{-1}. The background noise was collected simultaneously to the specularly reflected signal with a ^{3}He counter offset from the specular position by 0.44° towards larger scattering angles. It was directly subtracted from the specular signal to obtain the background corrected intensity. At small angles the samples were over-illuminated and therefore

the reflectivity data were footprint corrected for the varying flux on the sample as α increased and normalized to the measured incident intensity to obtain the reflectivity $R(Q_z)$.

The solutions were filled into the cells through access holes in the bottom of troughs which could be closed with Nylon screws. Since the solutions were flow-birefringent, prior to the measurement they were allowed to relax for at least three hours and up to 30 hours in the case of the solutions with the highest polymer volume fractions. For this reason it was not possible to record reflectivity data for proteated polymers in D_2O with volume fractions higher than ϕ=0.067. For the deuterated diblock copolymer in null reflecting water the accessible range of volume fractions was $\phi \leq 0.059$.

Results and Discussion

Binary mixtures of h-PB1,4-h-PEO in D_2O and of d-PB1,4-d-PEO in null reflecting water are permanently birefringent at volume fractions at which the solutions are in the nematic state. The location of the isotropic to nematic phase transition in the bulk was determined by visual inspection of the solutions between crossed polarizers. In neither case we could observe a complete macroscopic separation of the coexisting phases but the solutions of the proteated sample in H_2O were completely isotropic at volume fractions $\phi \leq 0.078$ and the solutions with the deuterated polymer in null reflecting water showed birefringent speckles above $\phi > 0.06$.

The different phase behavior hints at a significant difference in the morphology of the micelles, which form the nematic phase. This is actually expected as the PEO-block length of the deuterated sample is larger than that of the proteated polymer. The micellar morphology depends very subtly on the ratio of the respective block length [25,26,30]. It is thus essential to determine the micellar shape for the two polymers, prior to the investigation of the phase behavior close to an interface. To this end we performed static light scattering and small-angle neutron scattering experiments.

For solutions of the proteated polymer in H_2O with concentrations up to $c = 5.25\times10^{-3}$ g/mL we determined the zero scattering vector structure factor $S(Q=0)$ by linear least squares fitting of $1/M_{app}$

vs. c. From the low concentration data at $c \leq 2\times10^{-4}$ g/mL we extracted the mass average molar mass $M_w=(1.6\pm0.1)\times10^8$ g/mol of the micelles and the second osmotic virial coefficient $A_2=(8\pm1)\times10^{-6}$ mLg^{-1}mol^{-1}.

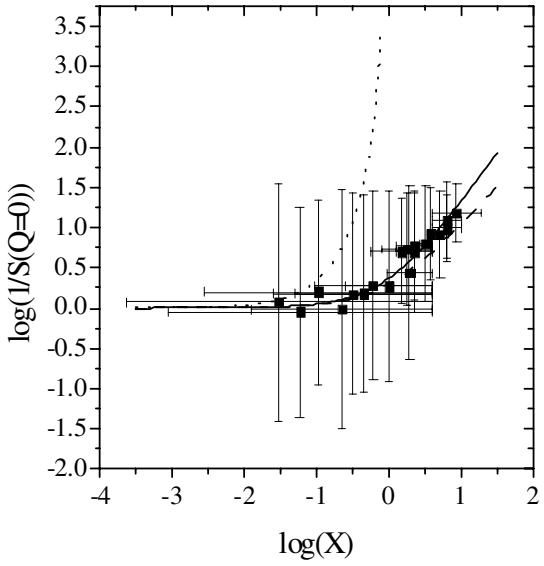

Figure 1 Inverse zero angle structure factor $S(Q=0)^{-1}$ versus reduced concentration $X=2A_2M_wc$. Symbols are experimental data from solutions of proteated h-PB1,4-h-PEO in H_2O and the lines are theoretical predictions for solutions of hard spheres (dotted), semi-flexible polymer chains (full) and hard rods (dashed). The error bars represent the uncertainties resulting from the linear least squares fitting of the SLS data.

In Fig.1 $S(Q=0)^{-1}$ is plotted versus the reduced concentration $X=2A_2M_wc$ on a double logarithmic scale. The errors represent the uncertainty of the linear least squares fitting of $1/M_{app}$ vs. c. In this representation $S(Q=0)^{-1}$ is sensitive to the particle shape[35], as is visualized by the theoretical curves for hard spheres[48,49], semi-flexible polymer chains[50] and hard rods[9], which are displayed for comparison. Despite the large experimental uncertainties, it is obvious from Fig. 1 that the micelles are non-spherical. However, it is not possible to distinguish from these data whether the micelles behave like hard rods or as semi-flexible cylinders, nor is any information about the micelles' cross-sectional dimensions available from SLS.

Therefore we performed SANS-experiments at concentration of 1mg/mL at which the structure factor of the solution $S(Q)$ is only insignificantly different from unity according to the light scattering

experiments. In Fig. 2 the radially averaged scattered intensities corrected for solvent and background scattering are plotted versus the scattering vector *Q*.

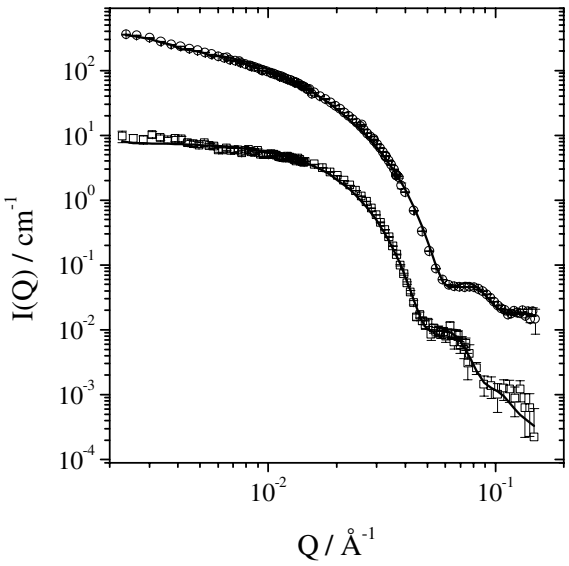

Figure 2 SANS-curves from aqueous solutions of PB-PEO block copolymers with a concentration of c=1 mg/mL. The open circles are data from the proteated diblock in D_2O, while the open squares are data from the deuterated polymer in null reflecting water. The latter is displaced on the ordinate by a factor of 0.1 for clarity. The full lines are best fits of the model described in the text.

We attempted to fit the experimental data with the model function for rigid cylinders with a Gaussian distribution of cross section radii, as it was suggested by Won et al. [29] for micelles of PB1,2-PEO block copolymers which had block lengths and PB-microstructure different from the block copolymers used in this study. However we were not able to get satisfactory results with this approach, especially the low q—part of the scattering curves could not be fitted, while the high q—part which is due to the cross section scattering was reproduced reasonably well. A closer look to the micrographs presented in the contribution by Won et al [29] reveals that the micelles exhibit a remarkable flexibility Therefore we used a model function for semi-flexible cylinders to fit the SANS data, which we had developed recently[37] along the ideas of Pedersen et al. [36]. If the length scale of the cylinders contour length, L_c, and its cross-section radius, R_{cs}, are sufficiently separated, the finite cross-section diameter of the cylinders can be taken into account by multiplying Koyama's expression for

the particle scattering factor of a polydisperse wormlike chain [39], $P_{wlc}(Q,L_c,b,U)$, with the cross-section form factor of a rigid homogeneous cylinder $P_{cs}(Q,R_{cs})$, i.e.

$$P(Q,L_c,b,U,R_{cs}) = P_{wlc}(Q,L_c,b,U)P_{cs}(Q,R_{cs}), \quad (2)$$

where b is the statistical Kuhn segment length, U is the polydispersity index of the contour length and

$$P_{cs}(Q,R_{cs}) = \left[\frac{2J_1(QR_{cs})}{QR_{cs}}\right]^2 \quad (3)$$

where R_{cs} is the cross-section radius and $J_1(QR_{cs})$ is the first order Bessel function. In the fitting algorithm the model function of eq. (2) was multiplied by an amplitude $I(Q=0)$ and data-smearing with a Gaussian-type resolution function as suggested by Pedersen [51] was taken into account. Although we took into account experimental data smearing, the minima in the scattering curves could not be reproduced properly by this model. Especially in the case of the deuterated polymer in non reflecting water the minima were much too sharp and to deep. As already discussed above this part of the curves could be well fitted with a model which accounts for polydispersity of the cross section diameter. Consequently, we further modified our model function, taking into account a Gaussian distribution of cross section radii. This procedure is rather time consuming, since $P_{wlc}(Q,L_c,b,U)$ contains two integrations, which can only be solved numerically [39,52], and two further numerical integration are required, one to account for the distribution of the cross section and another for experimental smearing. In order to reduce computer time, the polydispersity index was fixed to U=2.The full lines in Fig. 2 are the best fits of this model to the experimental data and the resulting parameter values are summarized in Table 2.

Table 2 Mean contour length, L_c, Kuhn segment length, b, mean cross-section radius, R_{cs} and its variance σ_{RCS} of the block copolymer micelles determined by non linear least squares fitting of the model function to SANS-data as described in the text.

Block copolymer	L_c / Å	b / Å	R_{cs} / Å	σ_{RCS}
h-PB1,4-h-PEO	3800± 100	59±15	67±2	0.15
d-PB1,4-d-PEO	590±70	70±15	83±2	0.09

We note that the over-all micellar contour length, $L_{c,}$ of the deuterated polymer is significantly smaller than in the case of the proteated polymer while R_{gcs} is larger for the deuterated micelles due to the higher degree of polymerization of the unimer PEO block (see Table 1). Consequently the aspect ratio is smaller in the case of the deuterated micelle, which corresponds to a higher mean curvature of the hypothetic plane that separates the hydrophobic core from the aqueous surroundings. This is well in line with other experimental findings [25,26,30] and the concept of spontaneous curvature of amphiphilic films[53].

To study the influence of a hard wall on the N/I phase transition we performed neutron reflectivity scans from the interface between a silicon single crystal and solutions of PB1,4-PEO block copolymers at two different scattering contrasts. The normalized reflectivity curves of a series of solutions containing proteated polymer dispersed in D_2O are plotted in the top of Fig. 3a as $R(Q_z)/R_F(Q_z)$ vs. Q_z

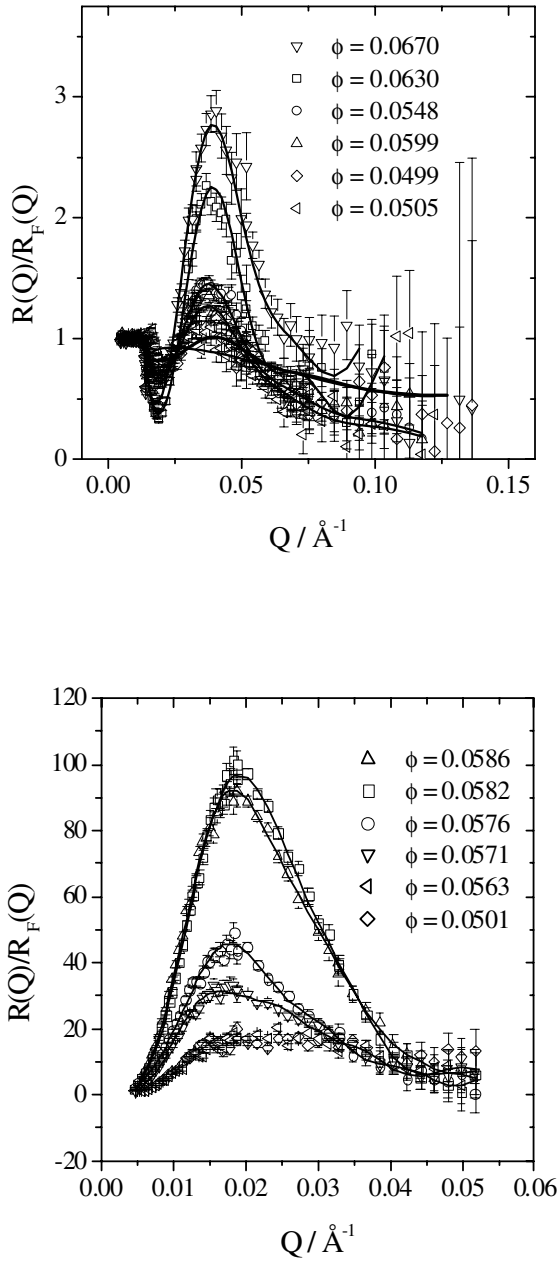

Figure 3 Normalized reflectivity data from an interface between a Si-single crystal and solutions of h-PB1,4-h-PEO in D_2O (top) and d-PB1,4-d-PEO in null reflecting water (bottom) respectively. The volume fractions of the solutions are indicated in the legends.

where $R_F(Q_z)$ is the theoretical Fresnel-reflectivity from a perfectly flat interface between the silicon and a fictitious solution with the same scattering length density, ρ, as the mean bulk value of the investigated solution. In this representation, the reflectivity from a perfectly smooth interface between two half-spaces would yield unity throughout the whole range of scattering vectors, if the scattering length densities of both half-spaces were constant up to the interface (z=0). In a real experiment the curve would slightly decay with increasing Q_z as the reflectivity is damped by the intrinsic roughness of the interface. However, if there is a thin layer at the interface which has a scattering length density different from the bulk value, the normalized reflectivity curve shows undulations. The periodicity of the undulations is inversely proportional to the thickness of the layer, and their amplitude is proportional to the scattering length density of the layer. All experimental curves in Fig. 3 a show a maximum region where $R(Q_z)/R_F(Q_z)>1$, which is very shallow at volume fractions $\phi<0.06$. Above this volume fraction the maximum value increases by a factor of about three in a very narrow regime while the position of the maximum does not change. The same features, although more pronounced, can be seen in Fig. 3b where the data from solutions of deuterated polymer in null reflecting water are shown. Here the $R(Q_z)/R_F(Q_z)$-curves for the two lowest volume fractions are indistinguishable with a maximum value of ca. 20. Then the maximum value increases up to roughly 100 in the very narrow range of $0.0563<\phi<0.0582$, while the position of the maximum remains unchanged. Upon further increase of the volume fraction the maximum value remains constant as well. This shows unambiguously that a layer is formed close to the interface at volume fractions $\phi>0.057$ in the case of the deuterated polymer in null reflecting water and above $\phi>0.06$ for the proteated polymer in D_2O. In both cases, the scattering length density of this layer is different from the bulk value of the solution, ρ_{bulk}, and it varies strongly with the bulk volume fraction, while the average thickness of the layer is invariant. These observations are strong evidence for the formation of an interfacial region which is nematically pre-ordered, since the number density of the polymer is higher in the nematic phase than in the isotropic solution.

To get a more quantitative picture of this interfacial layer we determined the scattering length density profiles from the reflectivity curves. This is an inverse problem, for which various solution strategies have been proposed [54]. Here we applied a two step strategy. First we used a model independent method (GTM-SA) [7] which combines the so called groove tracking method [41] with the simulated

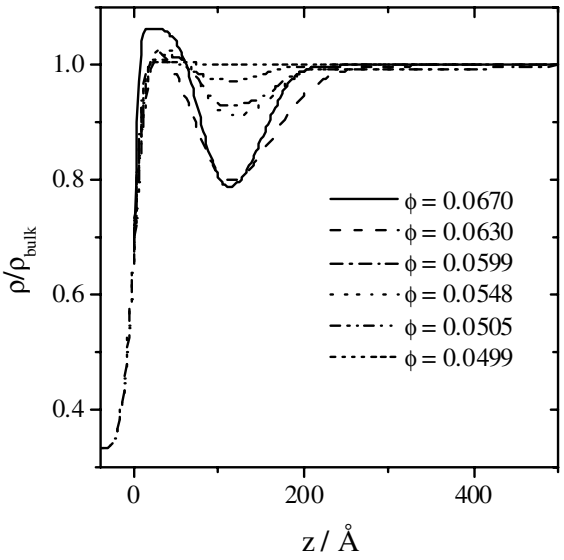

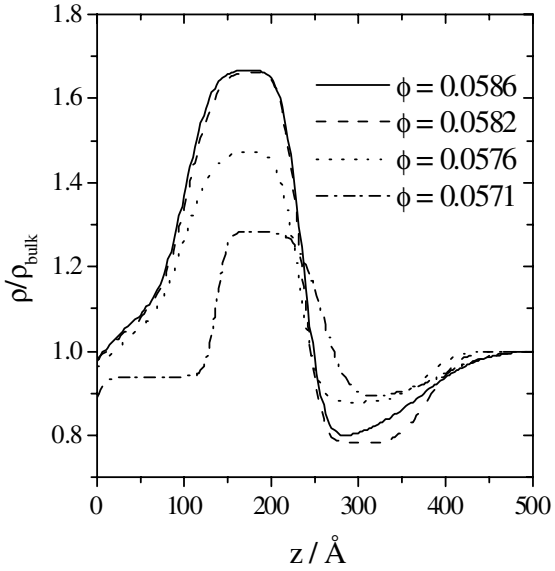

Figure 4 Normalized scattering length density profiles of an interface between a Si-single crystal and solutions of h-PB1,4-h-PEO in D_2O (top) and d-PB1,4-d-PEO in null reflecting water (bottom) respectively. The volume fractions of the solutions are indicated in the legends.

annealing technique [55]. The profiles obtained by GTM-SA were used to estimate reasonable starting values for the fitting of a multi-box (or slab) model [43]to the experimental data.

The results are displayed graphically in Fig. 4. In the case of deuterated polymers in null reflecting water, we were not able to get any reasonable fits at polymer volume fractions $\phi<0.0571$, due to the low signal to noise ratio of the experimental data. For the same reason we could not get reasonable reflectivity data at $q_{max}>0.05$ Å^{-1} from the deuterated polymer in null reflecting water (see also experimental section). This limits the spatial resolution of the experiment to distances larger than $\Delta d_{min}=2\pi/q_{max}\approx125$ Å. We will therefore not discuss the profiles displayed in Fig. 4 in detail, except for the observations that thickness of the region where the scattering length density deviates from the bulk value, d, is in the order of a few micellar segment lengths, b, as determined by SANS and not in the order of the contour length L_c. Further, we note that d is independent of the bulk volume fraction within the resolution of the experiment.

This observation is in contradiction to the theoretical predictions for the interface induced I/N pretransition of a hard rod system [10,11]. There it is expected that hard rods form a nematically pre-ordered phase next to a wall at $\phi_i\approx0.85\times\phi_{I/N}$. However, the thickness of this layer should initially be of the order of the rod length. In the light of the high flexibility of the micelles this discrepancy is not surprising. One would rather expect the micelles to behave like semi-flexible main chain liquid crystalline polymers. In this model the mesogenic entities can be identified with the Kuhn-segments of the chain.

With the approximation that the Kuhn-segments may be treated as Onsager-rods ($b>>R_{cs}$) Chen et al [12,13] calculated the segment density profile perpendicular to a wall using a density functional theory.

Like the theory for hard rods, this theory also predicts an interfacial pre-transition at roughly $\phi_i \approx 0.8 \times \phi_{I/N}$. However, the thickness of the pre-ordered layer is expected to be initially of the order of the Kuhn-length, b, and a significant increase of the thickness is only expected for $\phi > 0.99 \times \phi_{I/N}$. Accordingly our experimental observation that the thickness of the nematic layer is of the order of a few segment lengths may be regarded as qualitative agreement with the prediction by Chen et al. The fact that we did not observe the predicted divergence of the layer thickness is due to technical reasons. Solutions with $\phi > 0.9\phi_{I/N}$ show strong flow birefringence, which, if not relaxed, might mimic nematic ordering in the experiments. Since the relaxation times exceeded 30 hours it was not practical to collect more reflectivity data in this range of polymer volume fractions. We can therefore not distinguish whether the nematic layer wets the interface or not. In any case, the agreement with the theoretical prediction has to remain on a qualitative level because the segments of our block copolymer-micelles have a finite aspect ratio, while the theory assumes that $b >> R_{cs}$.

Conclusions

We have synthesized amphiphilic block copolymers by anionic polymerization, which form cylindrical micelles in aqueous solutions. The structural parameters of these micelles were determined by SANS. Despite the high flexibility of the micelles, their solutions form a nematic phase at sufficiently high polymer volume fractions. The influence of a hard wall on the formation of the nematic phase was studied by neutron reflectivity. From the reflectivity data it can be seen without any detailed analysis that the isotropic to nematic transition is shifted to lower volume fractions in a layer close to the wall. The thickness of this layer does not depend on the bulk volume fraction of the polymer, ϕ, while its density increases drastically with increasing ϕ. The quantitative analysis of the of the reflectivity data in terms of scattering length density profiles confirm these observation. Further, the thickness of the nematic layer is found to be of the order of a few Kuhn-segment lengths of the micelles. In particular this last finding shows that the behavior of the block copolymer micelles close to a wall can not be described by the theory for hard rods [10,11]. We rather find that our experimental

observations are in qualitative accord with the predictions by Chen et al [12,13] for a nematic pre-transition close to a wall for semi-flexible polymers. Since this theory is based on the assumption that the segments can be treated as Onsager-rods, a quantitative agreement with the experiment can not be expected. To remove this deficiency we are currently setting up a simulation scheme which takes into account the finite aspect ratio of the segments.

Acknowledgement The authors thank Gerd Meier for his help with the SANS experiments, Johan Buitenhuis and Zvonimir Dogic for their assistance with the reflectivity measurements, Jörg Stellbrink for giving access to the light scattering apparatus and the Berlin Neutron Scattering Center (BENSC) for the reflectivity beam time.

References

[1] Earnshaw, J. C.; Hughes, C. J. *Phys. Rev. A* **1992**, *46,* R4494.

[2] J. Als-Nielsen, F. Christensen, P. S. Pershan *Phys. Rev. Lett*. **1992,** *48*, 1107.[3] Ocko, B. M.; Wu, X. Z.; Sirota, E. B.; Sinha, S. K.; Gang, O.; Deutsch, M. *Phys. Rev. E* **1997**, *55*, 3164.

[4] Deutsch, M.; Wu, X. Z.; Sirota, E. B.; Sinha, S. K.; Ocko, B. M.; Magnussen, O. M. *Europhys. Lett*. **1995**, *30*, 283.

[5] Hayami, Y.; Findenegg, G. H. *Langmuir* **1997**, *13*, 4865.

[6] Gang, O.; Ellmann, J.; Möller, M.; Kraack, H.; Sirota, E. B.; Ocko, B. M.; Deutsch, M. *Europhys. Lett*. **2000**, *49*, 761.

[7] Marczuk, P.; Lang, P.; Findenegg, G. H.; Metha, S. K.; Möller, M. *Langmuir* **2002,** *18,* 6830.

[8] Lucht, R.; Marczuk, P.; Bahr, C., Findenegg, G. H. *Phys. Rev. E* **2001**, *63*, 41704.[9] Onsager, L. *Ann. New York Acad. Sci.* **1949**, *51*, 627.

[10] van Roij, R; Dijkstra, M.; Evans, R. *J. Chem. Phys*. **2000**, *113*, 7689.

[11] Dijkstra, M.; van Roij, R; Evans, R. *Phys. Rev. E* **2001**, *63*, 1703.

[12] Cui, S. M.; Akcakir, O.; Chen, Z. Y. *Phys. Rev. E* **1995**, *51*, 4548.

[13] Chen, Z. Y.; Cui, S. M. *Phys. Rev. E* **1995**, *52*, 3876.

[14] Lang, P. *J. Phys. Chem B* **1999,** *103,* 5100.

[15] Madsen, A.; Konovalov, O.; Robert, A.; Grübel. G, *Phys. Rev. E* **2001** *64*, 061406.

[16] Förster, S.; Hermsdorf, N.; Leube, W.; Schnablegger, H.; Regenbrecht, M.; Akari, S.; Lindner, P.; Böttcher, C. *J. Phys. Chem. B* **1999**, *103*, 6657.

[17] Regenbrecht, M.; Akari, S.; Förster, S.; Möhwald, H. *J. Phys. Chem. B* **1999**, *103*, 6669.

[18] Alexandridis, P.; *Curr. Opinion Coll. Inter. Sci.* **1997**, *2*, 478.

[19] Alexandridis, P; Lindman, B. Eds. "*Amphiphilic Block Copolymers: Self Assembly and Application*" Elsevier, New York 2000.

[20] Cameron, N. S.; Corbierre, M.; Eisenberg, A. *Can. J. Chem.* **1999**, *77*, 1.

[21] Zhang, L.; Eisenberg, A. *Science* **1995**, *268*, 1728.

[22] Yu, K.; Zhang, L.; Eisenberg, A. *Langmuir* **1996**, *12*, 5980.

[23] Burke, S. Eisenberg, A. *High Perf. Polym.* **2000**, *12*, 535.

[24] Deng, Y.; Young, R. N.; Rayn, A. J.; Fairclough, J. P. A.; Norman, A. I.; Tack, R. D. *Polymer* **2002**, *43*, 7155.

[25] Willner, L.; Poppe, A.; Allgaier, J.; Monkenbusch, M.; Lindner, P.; Richter, D. *Europhys. Lett*. **2000**, *51*, 628.

[26] Kaya, H. PhD-thesis Universität Münster, Germany, 2003

[27] Poppe, A.; Willner, L.; Allgaier, J.; Stellbrink, J.; Richter, D. *Macromolecules* **1997**, *30*, 7462.

[28] Kaya, H.; Willner, L.; Allgaier, J.; Stellbrink, J.; Richter, D. *Appl. Phys. A* **2002**, *74*, 499

[29] Won, Y. Y.; Davis, H. T.; Bates, F. S. *Science* **1999**, *283*, 960.

[30] Hentze,H. P.; Krämer, E.; Berton,B.; Förster, S.; Antonietti, M.; Dreja, M. *Macromolecules* **1999**, *32*, 5803.

[31] Egger, H.; Nordskog, A.; Lang, P.; Brandt, A. *Macromol. Symp.* **2000**, *162*, 291.

[32] Nordskog, A.; Egger, H.; Findenegg, G. H.; Schlaad, H.; von Berlepsch, H.; Böttcher, C. *Phys. Rev. E* in press.

[33] Jain, S.; Bates, F. S. *Science* **2003**, *300*, 460.

[34] Zimm, B. H. J. *Chem. Phys*. **1948**, *16*, 1093

[35] Burchard W. in *Light Scattering: Principles and Development* (Brown, W., Ed.), Clarendon Press, Oxford, 1996.

[36] Pedersen, J. S.; Schurtenberger, P. *Macromolecules* **1996,** *29,* 7602.

[37] Menge, U.; Lang, P.; Findenegg, G. H.; Strunz, P. *J. Phys. Chem. B* **2003,** *107,* 1316.

[38] Kuhn, W.; Kolloid Z. **1934**, *68*, 2.

[39] Koyama, R. *J. Phys. Soc. Japan* **1973**, *34* 1029.

[40] Thomas, R. K. in *Modern Characterization Methods of Surfactant Systems; Surfactant Science Series* **83** (Binks, B.P., Ed.), Marcel Dekker Inc., New York, 1999.

[41] Zhou, X. L.; Chen, S. H. *Phys. Rev. E* **1993,** *47*, 3174.

[42] Pedersen, J. S. *J. Appl. Cryst.* **1992**, *25*, 129.

[43] Als-Nielsen, J.; Jacquemain, D.; Kjaer, K.; Leveiller, F.; Lahav, M.; Leiserowitz, L. *Physics Reports* **1994**, *246*, 251.

[44] Allgaier, J.; Poppe, A.; Willner, L.; Richter, D. *Macromolecules*, **1997**, *30*, 1582.

[45] Menge, U.; Lang, P.; Findenegg, G. H . *J. Phys. Chem. B* **1999,** *103*, 5768.

[46] Pyckhout-Hintzen, W.; Springer, T.; Forster, F.; Gronski, W.; Fischkorn, C. *Macromolecules* **1991**, *24*, 1269.

[47] Mezei, F; Goloub, R; Klose, F; Toews, H. *Physica B* **1995**, *213/214*, 898.

[48] Percus, J. K.; Yevick, G. J.; *Phys. Rev.* **1958**, *110*, 1.

[49] Carnahan, N. F.; Starling, K. E. *J. Chem. Phys.* **1969**, *51*, 635.

[50] Ohta, T.; Oono, Y. *Phys. Lett.* **1982**, *89A*, 460.

[51] Pedersen, J. S. *J. Appl. Cryst* **1990**, *23* 321.

[52] Schmidt, M.; *Macromolecules* **1984**, *17*, 553.

[53] see for example Israelachvili, J. N. “Intramolecular and Surface Force”, Academic Press London 1985.

[54] for an overview see Lovell, R. M.; Richardson, R. M. *Curr. Opin. Colloid Interf. Sci.* **1999,** *4*, 197.

[55] Kirkpatrick, S.; Gelatt, C.O.; Vecchi, M.P. *Science* **1983**, *220*, 671.